

**Design for Multi-step Mechanochromic Luminescent  
Property by Enhancement of Environmental Sensitivity in  
the Solid-state Emissive Boron Complex**

|                               |  |
|-------------------------------|--|
| Journal:                      | <i>Materials Chemistry Frontiers</i>   |
| Manuscript ID                 | QM-RES-11-2019-000719.R2   |
| Article Type:                 | Research Article   |
| Date Submitted by the Author: | 27-Feb-2020  |
| Complete List of Authors:     | Saotome, Satoru; Kyoto University<br>Suenaga, Kazumasa; Kyoto University, Polymer Chemistry<br>Tanaka, Kazuo; Kyoto University, Polymer Chemistry<br>Chujo, Yoshiki; Kyoto University, Polymer Chemistry |
|                               |  |

# Design for Multi-step Mechanochromic Luminescent Property by Enhancement of Environmental Sensitivity in the Solid-state Emissive Boron Complex

*Satoru Saotome, Kazumasa Suenaga, Kazuo Tanaka\* and Yoshiki Chujo*

Department of Polymer Chemistry, Graduate School of Engineering, Kyoto

University,

Katsura, Nishikyo-ku, Kyoto 615-8510, Japan

E-mail: [tanaka@poly.synchem.kyoto-u.ac.jp](mailto:tanaka@poly.synchem.kyoto-u.ac.jp)

Phone: +81-75-383-2604

Fax: +81-75-383-2605

**KEY WORDS:** mechanochromism, solid-state luminescence, boron, crystal polymorph



## ABSTRACT

We have recently reported multi-state emission of the fused boron ketoiminate (FBKI) complexes and their mechanochromic luminescent behaviors. Based on this structure, we introduced the thienyl unit for improving molecular planarity and facilitating intermolecular electronic conjugation in order to enhance stimuli responsiveness luminescent chromism in the solid state. It was found that the synthesized complex (FBKI-thio) can form two types of crystal polymorphs and their mechanochromic luminescent behaviors. The green-emissive polymorph (crystal **A**) shows typical peak shift triggered by grinding the crystalline powder sample, meanwhile the orange-emissive one (crystal **B**) exhibits multi-step luminescent chromism. By tapping, the new two peaks appeared in the shorter wavelength region in photoluminescence spectrum, and intensities of these emission bands were enhanced by additionally grinding. From the lifetime measurements, it was revealed that new energy levels should be generated after the mechanical treatments. By applying tender mechanical forces, collapses of regular structures could be partially induced, and subsequently the amorphous states should be realized by the following strong forces. It is proposed that FBKI-thio is able to sensitively detect these morphology changes in solid and present different luminescent color because of enhanced planarity and electronic conjugation. We also mention that the applied physical forces can be evaluated from the changes in intensity ratios between these emission bands.

## INTRODUCTION

The molecules with mechanochromic luminescent properties have attracted tremendous attention as a platform of a chemical sensor for monitoring external forces applying to products.<sup>1-8</sup> For example, by using these molecules as a sensor, vital signs, such as vascular flow, can be monitored in real time.<sup>9</sup> Such information would be helpful for establishing daily health care system. Additionally, pressures and distortions are able to be evaluated from the optical property changes.<sup>10-12</sup> Therefore, much effort has been devoted to discover the key skeletons possessing wide applicability as a stimuli-responsive material as well as mechanochromic luminescent property.<sup>13-23</sup> However, there are still difficulties for meeting the demands based on the single type of organic molecules for realizing stimuli-responsive luminescent chromism with high sensitivity toward weak forces. Most of luminescence properties from conventional dyes are often spoiled in the condensed state due to concentration quenching caused by non-specific intermolecular interactions. Furthermore, although concentration quenching can be suppressed through inhibition of intermolecular interactions by introducing bulky substituents around the chromophore units<sup>24-27</sup> or by wrapping emissive molecules by the transparent matrices<sup>28</sup> to isolate chromophores from neighboring molecules, the resulting solid-state luminescent molecules tend to be insensitive toward environmental changes. Hence, the limited numbers of the design strategies are available for obtaining small-type of molecules having mechanochromic luminescence.

Boron complexes have been paid attention as a platform for developing solid-state luminescent materials with stimuli-responsiveness because of superior intrinsic

luminescent properties, such as large light-absorption ability, intense luminescent property and tunability of optical characters by chemical modification.<sup>29</sup> The small number of molecules can avoid concentration quenching and very few showed luminescent chromism without decreases in luminescent properties by applying mechanical forces to their solid samples. In the previous examples, the most common mechanism is based on structural transitions between crystal and amorphous phases.<sup>30</sup> By adding mechanical forces into the crystalline samples, regular structures are collapsed, followed by significant changes in molecular distributions. Finally, mechanochromic luminescence can be induced through the alteration of degree of intermolecular interactions. We have also found that the class of boron complexes presenting large degree of structural relaxation in the excited state can show aggregation- and/or crystallization-induced emission properties.<sup>31</sup> By utilizing these skeletons as an “element-block”,<sup>32,33</sup> which is defined as a minimum functional unit consisting of heteroatom, solid-state luminescent conjugated materials and polymers have been developed.<sup>34-42</sup> In particular, based on the strategy for preserving solid-state luminescent property of boron ketoiminate,<sup>43,44</sup> we designed the fused structure and observed multi-state constant emission intensity as well as mechanochromic luminescence.<sup>45,46</sup> Next, we sought to evolve mechanochromic luminescent properties.

Herein, we report multi-step mechanochromic luminescence from rationally-designed thiophene-connected fused boron ketoiminate (FBKI, Scheme 1). By varying solution components in recrystallization, green and orange-emissive crystalline polymorphs were obtained. Both samples showed mechanochromic luminescence. Interestingly, by adding weak mechanical forces by tapping to the crystalline sample with orange

emission, luminescent chromism to yellow was observed. Consequently, green emission was detected by applying stronger forces through grinding treatments. From the deconvolution of peak shapes, it was revealed that the luminescence spectra in the solid state of the complex are composed of three independent emission bands. By adding mechanical forces, alteration of the existence ratio of these chromophores occurred, resulting in multi-step luminescent chromism. This is the first example, to the best of our knowledge, to offer luminescent chromism originated by the generation of different kinds of chromophores by physical forces without chemical degradation.

## RESULTS

Boron ketoiminates<sup>43,44</sup> possessing aggregation-induced emission (AIE) properties are regarded as a versatile element-block for obtaining stimuli-responsive solid-state luminescent materials, and indeed the series of chemical sensors have been developed. Recently, we have reported multi-state emission of the boron ketoiminate derivatives.<sup>45,46</sup> By introducing the fused structure<sup>47–57</sup> at the nitrogen atom in the ketoiminate ligand, we expected that molecular motions should be effectively suppressed.<sup>58,59</sup> Therefore, excitation deactivation due to intramolecular motions is likely to decrease. As a result, fused boron ketoiminates show constant emission efficiencies in the solid state, such as the amorphous and crystal forms, as well as in solution. Moreover, the fused boron ketoiminates showed luminescent chromism originated from changes in intermolecular interaction. Based on these results, we sought to realize multi-step luminescent chromism by applying external forces. By replacing the phenyl group to the thienyl ring, high planarity and strong intermolecular interaction could be enhanced.<sup>60</sup> Consequently, optical properties could be sensitively influenced by molecular environmental alterations induced by morphology changes.

The synthetic protocols for thienyl fused boron ketoiminate (FBKI-thio) are shown in Scheme 1. After the Suzuki–Miyaura cross coupling reaction, the desired product, FBKI-thio was obtained as a yellow powder (crystal **A**) from recrystallization. The chemical structure of the product was examined with <sup>1</sup>H, <sup>11</sup>B and <sup>13</sup>C NMR spectroscopies (Charts S1–S6), high-resolution mass measurement, elemental analysis, and X-ray crystallography, and it was confirmed that the desired molecule can be



obtained. The products showed good stability under air even against heating and solubility in common organic solvents such as chloroform, dichloromethane and tetrahydrofuran (THF). From these data, we concluded that the products had enough stability for following optical measurements. Intense emission was presented both in solution and solid. From the optical measurements in THF, the absorption and emission bands were observed in relatively-longer wavelength regions from FBKI-thio than those from FBKI (Figure S1, Table S1).<sup>45</sup> From the data from cyclic voltammetry and quantum calculations (Table S2, Figure S2), elevation of energy level of highest occupied molecular orbital (HOMO) was observed from FBKI-thio, suggesting that electronic conjugation should be developed because of strong electron-donating ability of thiophene than that of benzene. When FBKI-thio was recrystallized from methanol at 50 °C, the orange crystal (crystal **B**) was obtained. In other cases where common organic solvents such as THF, chloroform and so on are used as a solvent, only crystal **A** was obtained. Since the identical <sup>1</sup>H NMR spectra were obtained between crystals **A** and **B**, we concluded that crystal polymorphs can be separately prepared by selecting the type of solvents in recrystallization.

### Scheme 1

Intense emission was observed from both crystals. To evaluate optical properties, photoluminescence (PL) spectra were initially measured (Figure 1). The emission band of crystal **A** was observed in the green region with the peak at 500 nm. In the PL spectrum of crystal **B**, the emission band appeared in the longer wavelength region ( $\lambda_{em,max} = 566$  nm) than that of crystal **A**. It should be noted that such large difference in

the maximum wavelengths of emission bands is very rare in the crystal polymorphs. Initially, from the  $^1\text{H}$  NMR measurements with both crystals, It is clearly shown that both crystals include no solvent molecules, meaning that this large degree of difference might be originated from different packing structures and strengths of intermolecular interactions (Figure S3). Indeed, much higher thermal stability and melting temperature were detected from crystal **A** (Figure S4, Table S3). Fortunately, the packing structure of crystal **A** was determined by X-ray crystallography (CCDC #1957640) and compared to that of FBKI, while crystal **B** was not applicable for the analysis due to fragility (Figures S5 and S6, Table S4). Accordingly, it was shown that FBKI-thio has high planarity and tight packing than FBKI as we expected. In strongly-packed crystals, stabilization effects can be often obtained by large overlaps of molecular orbitals.<sup>61</sup> Thus, it is speculated that crystals of FBKI-thio might include stronger  $\pi$ - $\pi$  interaction than those of FBKI. According to phase-transition temperatures obtained from DSC data, crystal **A** has higher values (Table S3). In crystal **A**, stacking, which generally plays a significant role in the improvement of thermal stability, was confirmed according to X-ray crystallography. On the other hand, since crystal **B** shows high sensitivity toward external stimuli as mentioned later, it is implied that intermolecular interaction could be hardly obtained. Therefore, larger degree of structural relaxation should be acceptable in the excited state. Thus, the emission band could appear in the longer wavelength region. This speculation might be supported by the fact that lower phase-transition temperatures were detected from crystal **B**.

Figure 1

Next, mechanochromic luminescent behaviors of both crystals were investigated (Figure 1). The crystalline samples were ground in an agate bowl, and changes in emission color were monitored. Both crystals **A** and **B** clearly showed luminescent chromism after applying mechanical stimuli basically to the blue-shifted color. Interestingly, crystal **B** displayed multi-step changes by smashing and subsequently grinding with the pile of crystal particles. Striking forces were applied to crystal **B** with a small bar such as a spoon until these particles were turned into much smaller pieces (named as B-smashed, **B-s**). The resulting **B-s** showed yellowish-green emission, which is obviously blue-shifted luminescent color compared with that of the pristine **B**. Continuously, when ground into the powder under additional large forces for a long time, the sample (named B-ground, **B-g**) showed further blue-shifted emission color. Overall, the two-step mechanochromic luminescence was observed in the transitions from crystal **B** (orange) to **B-s** (yellowish-green) by smashing and from **B-s** to **B-g** (yellow) by grinding.

The mechanochromic luminescent behaviors were analyzed with PL measurements (Figure 1, Table 1). We applied mechanical forces to the pristine samples until emission color changes were no longer detected. From crystal **A**, typical spectra were obtained. Before grinding, crystal **A** presented the unimodal emission band. Correspondingly, the blue-shift occurred by the grinding treatment for 10 min, and the unimodal band was detected in the shorter wavelength region from **A-g** (Figure S8a). By smashing, significant changes were hardly observed. In contrast, unexpected spectrum features were observed from crystal **B**. The initial sample of crystal **B** exhibited a unimodal spectrum. It should be noted that the multimodal shape with the peak and shoulders

around 480, 525 and 565 nm was observed from **B-s** by smashing for 5 min (Figure S8b). After grinding for additional 20 min to prepare **B-g**, the dual-modal spectrum with the peaks around 480 and 525 nm was obtained. **B-g** was also directly obtained by grinding the pristine **B**. The peak shifts have been usually observed from the organic mechanochromic luminescent dyes in the previous reports, similarly to crystal **A**. In contrast, isolated emission bands appeared in FBKI-thio. It is suggested that multiple states should be generated by the mechanical forces in the case of the orange-luminescent crystal of FBKI-thio. We also investigated reversibility by heating at 80 °C for 1 h and emission spectra and powder X-ray diffraction (P-XRD) were examined (Figures S9 and S10). From **A-g** and **B-g**, reversible changes to emission colors like **A** and **B-s** with partially **B** were observed once the samples were melted by heating, respectively. It is implied that molecular distributions might be preserved in the apparent melting state. In summary, it can be said that FBKI-thio has luminescent chromic materials.

Table 1

To obtain deep insight from the PL spectra, we performed the peak separation through the mathematical shape analysis. A peak is presumed to be a unimodal Gauss shape, and deconvolution was carried out for extracting each peak (Figure 2, Table 2). In the pristine crystals **A** and **B** and **A-g**, only the single peak was able to be obtained, meanwhile two significant peaks were obtained in the shorter wavelength region with the peaks at 529 and 490 nm from **B-s** and **B-g** than that at 560 nm in crystal **B**. Notably, the ratio of the peak area of the peak around 490 nm increased in **B-g**,

indicating that new energy states are able to be generated by applying the mechanical forces to crystal **B**. By changing the existing ratios among these species, multi-step luminescent chromism is induced.

#### Figure 2, Table 2

To support the above discussion regarding the generation of new species by the mechanical treatments, the emission lifetimes were estimated at the peak and shoulder wavelength positions (Tables 1 and S5, Figure S7). The most significant point is the generation of the new component in crystal **B** after the treatment. In the pristine crystal **B**, two components with relatively shorter lifetimes were observed at 566 nm, while the third component with the longer lifetime appeared in **B-s**. In particular, by changing the detection wavelength to 529 and 490 nm, larger and smaller proportions of the longer lifetime component and the shorter ones were observed, respectively. This tendency was much clearly exhibited in **B-g**, meaning that the new excited states, from which the shorter-wavelength emission bands with longer lifetimes are promised to be generated, are created by the mechanical treatments with **B**. In the case of crystal **A**, significant changes were hardly detected, indicating that luminescent chromism should be caused by the structural change from the regular structure to random distribution. According to the previous report on multi-step luminescent chromism with the boron complex, the mechanical treatment such as tapping generates defect sites, followed by collapse of crystalline packing.<sup>62</sup> Owing to high responsivity of FBKI-thio to environmental alterations, each step can be detected and different emission color was exhibited.

In the case of crystal **B**, the emission quantum yields were lowered, and shorter effects on each component were observed during the transitions not only from crystal **B** to **B-s** but also from **B-s** to **B-g**. Molecular mobility would be facilitated by losing regular structures in solid. Hence, decreases in lifetimes as well as emission quantum yields should be detected. Before and after the grinding treatment with crystal **A**, two components were obtained from the curve fitting, and similarly to crystal **B**, these two lifetimes were shortened by grinding. It is likely that molecular motions should be enhanced in the amorphous state caused by mechanical forces, followed by rapid decay in the excited state. Loss of the quantum yield supports this mechanism.

P-XRD measurements were performed to examine morphological changes of two crystal phase (Figure 3). Broader peaks were observed from **A-g** than that of crystal **A**, indicating that regular structures should be disrupted by mechanical stimuli. In crystal **B**, **B-s** showed new diffraction peaks except for those at the same positions with crystal **B**. It is likely that crystalline structures were gradually collapsed by mechanical stimuli, and new fracture surfaces could be generated by smashed. The molecules near these critical surfaces might provide the second component in the lifetime measurements. After the grinding treatment with **B-s**, some of new peaks disappeared and the same pattern to that of **A-g** was finally obtained. These common broad peaks at the same diffraction angles in the P-XRD patterns of **A-g** and **B-g** imply that that FBKI-thio could keep regular structures at the molecular level in both polymorphs even after strong grinding treatments. Therefore, the first components can be detected in the lifetime measurements. In summary, the multi-step mechanochromic behavior should be originated from gradual structural disruptions of crystal **B**. It is likely that tiny fraction

surfaces generated by smashing, followed by grinding should be included in **B-g**. Further, existence ratios of these fractions and amorphous, in which X-ray scattering hardly occurs, are also varied. Therefore, **B-g** showed different emission color from that of **A-g** although the same P-XRD pattern was apparently observed.

Figure 3

## DISCUSSION

The single-step luminescent chromism of crystal **A** is able to be explained by the characteristic crystal packing. Similarly to other boron complexes, the closely-packed structure was observed in crystal **A**. Therefore, it is likely that excitation deactivation caused from molecular vibrations can be efficiently suppressed by structural restriction.<sup>58,59</sup> Moreover, the emission bands tend to appear in the long wavelength region since energy levels received the stabilization effect originated from large overlaps of molecular orbitals. By adding mechanical forces to the crystalline samples, collapses and disordering of regular structures would be induced, leading to random distribution in which the stabilization effect critically decreased. As a result, degree of overlaps of molecular orbitals could be lowered in the disordered state. Finally, blue-shifted emission bands with smaller quantum yields were observed after grinding. In the multi-step behavior of crystal **B**, similar scenario can be proposed. The emission color changes by the mechanical stimuli are originated from changes of molecular distributions. When the crystal **B** with the tightly-packed structure is smashed, collapses partly occurred. The FBKI-thio molecules located around defects could show the new emission band at the shorter wavelength region. By applying stronger mechanical

forces, the proportion of disordered structures should be enhanced and correspondingly the emission band at much shorter-wavelength region became dominant. Consequently, the next luminescent chromism was detected. Not only solid-state luminescent property but also sensitivity toward environmental changes of FBKI-thio should play a key role in multi-step optical changes.

Luminescent color at each state can be depicted by the combination with two and three different kinds of emission bands of crystals **A** and **B**, respectively. From the calculation of intensity ratios at the peak wavelength in each mechanochromic state, clear difference was observed (Table 2). In particular, owing to three distinct components, crystal **B** enables us to describe emission properties as three kinds of intensity ratios. This demonstration could be applicable for the quantitation of applied mechanical forces to the products by using our luminescent dye as a coating-type indicator.

## CONCLUSION

Based on the multi-state luminescent FBKI skeleton, the solid-state luminescent boron complex with enhanced stimuli responsiveness was designed by introducing the thienyl unit for improving molecular planarity and electronic conjugation. The synthesized complex showed solid-state luminescence and two types of crystal polymorphs having mechanochromic luminescent properties. Especially, one of the crystal polymorphs exhibited multi-step luminescent chromism by tapping and subsequently grinding the powder sample. According to the peak deconvolution of PL



spectra and optical data, it is shown that different kinds of energy levels should be created by the mechanical treatments through gradual disruptions of tight crystalline structures. Our strategy to enhance planarity and electronic interaction in solid-state luminescent dyes could be versatile not only for obtaining stimuli-responsive optical materials with far higher sensitivity in subtle environmental alterations but also for unique luminescent chromic properties as shown here.

#### **ACKNOWLEDGMENT**

This work was partially supported by the Asahi Glass Foundation (for K.T.) and a Grant-in-Aid for Scientific Research (B) (JP17H03067) and (A) (JP17H01220) and for Challenging Research (Pioneering) (JP18H05356) and by Adaptable and Seamless Technology transfer Program through Target-driven R&D (A-STEP) from Japan Science and Technology Agency(JST).

## References

1. Y. Q. Dong, J. W. Y. Lam and B. Z. Tang, Mechanochromic Luminescence of Aggregation-Induced Emission Luminogens, *J. Phys. Chem. Lett.*, 2015, **6**, 3429–3436.
2. A. Pucci and G. Ruggeri, Mechanochromic polymer blends, *J. Mater. Chem.*, 2011, **21**, 8282–8291.
3. K. Ariga, T. Mori and J. P. Hill, Mechanical Control of Nanomaterials and Nanosystems, *Adv. Mater.*, 2012, **24**, 158–176.
4. A. Pucci, R. Bizzarri and G. Ruggeri, Polymer composites with smart optical properties, *Soft Matter*, 2011, **7**, 3689–3700.
5. X. Zhang, Z. Chi, Y. Zhang, S. Liu and J. Xu, Recent advances in mechanochromic luminescent metal complexes, *J. Mater. Chem. C*, 2013, **1**, 3376–3390.
6. P. Xue, J. Ding, P. Wang and R. Lu, Recent progress in the mechanochromism of phosphorescent organic molecules and metal complexes, *J. Mater. Chem. C*, 2016, **4**, 6688–6706.
7. Z. Ma, Z. Wang, M. Teng, Z. Xu and X. Jia, Mechanically Induced Multicolor Change of Luminescent Materials, *ChemPhysChem*, 2015, **16**, 1811–1828.
8. P.-Z. Chen, L.-Y. Niu, Y.-Z. Chen and Q.-Z. Yang, Difluoroboron -diketonate dyes: Spectroscopic properties and applications, *Coord. Chem. Rev.*, 2017, **350**, 196–216.
9. A. K. Bansal, S. Hou, O. Kulyk, E. M. Bowman and I. D. W. Samuel, Wearable Organic Optoelectronic Sensors for Medicine, *Adv. Mater.*, 2015, **27**, 7638–7644.

10. F. Ciardelli, G. Ruggeri and A. Pucci, Dye-containing polymers: methods for preparation of mechanochromic materials, *Chem. Soc. Rev.*, 2013, **42**, 857–870.
11. Z. Chi, X. Zhang, B. Xu, X. Zhou, C. Ma, Y. Zhang, S. Liu and J. Xu, Recent advances in organic mechanofluorochromic materials, *Chem. Soc. Rev.*, 2012, **41**, 3878–3896.
12. M. Gon, K. Kato, K. Tanaka and Y. Chujo, Elastic and mechanofluorochromic hybrid films with POSS-capped polyurethane and polyfluorene, *Mater. Chem. Front.*, 2019, **3**, 1174–1180.
13. F. Wang, C. A. DeRosa, M. L. Daly, D. Song, M. Sabat and C. L. Fraser, Multi-stimuli responsive luminescent azepane-substituted  $\beta$ -diketones and difluoroboron complexes, *Mater. Chem. Front.*, 2017, **1**, 1866–1874.
14. W. A. Morris, T. Butler, M. Kolpaczynska and C. L. Fraser, Stimuli responsive furan and thiophene substituted difluoroboron  $\beta$ -diketonate materials, *Mater. Chem. Front.*, 2017, **1**, 158–166.
15. T. Seki, K. Ida and H. Ito, A meta-diisocyanide benzene-based aryl gold isocyanide complex exhibiting multiple solid-state molecular arrangements and luminescent mechanochromism, *Mater. Chem. Front.*, 2018, **2**, 1195–1200.
16. T. Seki, N. Tokodai, S. Omagari, T. Nakanishi, Y. Hasegawa, T. Iwase, T. Taketsugu and H. Ito, Luminescent Mechanochromic 9-Anthryl Gold(I) Isocyanide Complex with an Emission Maximum at 900 nm after Mechanical Stimulation, *J. Am. Chem. Soc.*, 2017, **139**, 6514–6517.
17. Y. Sagara, M. Karman, E. Verde-Sesto, K. Matsuo, Y. Kim, N. Tamaoki, C. Weder, Rotaxanes as Mechanochromic Fluorescent Force Transducers in Polymers, *J. Am. Chem. Soc.*, 2018, **140**, 1584–1587.

18. M. Ikeya, G. Katada and S. Ito, Tunable mechanochromic luminescence of 2-alkyl-4-(pyren-1-yl)thiophenes: controlling the self-recovering properties and the range of chromism, *Chem. Commun.*, 2019, **55**, 12296–12299.
19. Y. Sagara, K. Kubo, T. Nakamura, N. Tamaoki and C. Weder, Temperature-Dependent Mechanochromic Behavior of Mechanoresponsive Luminescent Compounds, *Chem. Mater.*, 2017, **29**, 1273–1278.
20. R. Kaneko, Y. Sagara, S. Katao, N. Tamaoki, C. Weder and H. Nakano, Mechano - and Photoresponsive Behavior of a Bis(cyanostyryl)benzene Fluorophore, *Chem. Eur. J.*, 2019, **25**, 6162–6169.
21. B. Huang, W.-C. Chen, Z. Li, J. Zhang, W. Zhao, Y. Feng, B. Z. Tang and C.-S. Lee, Manipulation of Molecular Aggregation States to Realize Polymorphism, AIE, MCL, and TADF in a Single Molecule, *Angew. Chem. Int. Ed.*, 2018, **57**, 12473–12477.
22. G. Huang, Y. Jiang, S. Yang, B. S. Li and B. Z. Tang, Multistimuli Response and Polymorphism of a Novel Tetraphenylethylene Derivative, *Adv. Funct. Mater.*, 2019, **29**, 1900516.
23. F. Zhao, Z. Chen, C. Fan, G. Liu and S. Pu, Aggregation-induced emission (AIE)-active highly emissive novel carbazole-based dyes with various solid-state fluorescence and reversible mechanofluorochromism characteristics, *Dyes Pigm.*, 2019, **164**, 390–397.
24. C.-H. Zhao, A. Wakamiya and S. Yamaguchi, Highly Emissive Poly(aryleneethynylene)s Containing 2,5-Diboryl-1,4-phenylene as a Building Unit, *Macromolecules*, 2007, **40**, 3898–3900.
25. C.-H. Zhao, E. Sakuda, A. Wakamiya and S. Yamaguchi, Highly Emissive

- Diborylphenylene - Containing Bis(phenylethynyl)benzenes: Structure-Photophysical Property Correlations and Fluoride Ion Sensing, *Chem. Eur. J.*, 2009, **15**, 10603–10612.
26. X. Yin, F. Guo, R. A. Lalancette and F. Jäkle, Luminescent Main-Chain Organoborane Polymers: Highly Robust, Electron-Deficient Poly(oligothiophene borane)s via Stille Coupling Polymerization, *Macromolecules*, 2016, **49**, 537–546.
  27. H. Mori, K. Nishino, K. Wada, Y. Morisaki, K. Tanaka and Y. Chujo, Modulation of luminescence chromic behaviors and environment-responsive intensity changes by substituents in bis-o-carborane-substituted conjugated molecules, *Mater. Chem. Front.*, 2018, **2**, 573–579.
  28. M. Gon, K. Tanaka and Y. Chujo, Creative Synthesis of Organic–Inorganic Molecular Hybrid Materials, *Bull. Chem. Soc. Jpn.*, 2017, **90**, 463–474.
  29. K. Tanaka and Y. Chujo, Advanced Luminescent Materials Based on Organoboron Polymers, *Macromol. Rapid Commun.*, 2012, **33**, 1235–1255.
  30. G. Zhang, J. Lu, M. Sabat and C. L. Fraser, Polymorphism and Reversible Mechanochromic Luminescence for Solid-State Difluoroboron Avobenzene, *J. Am. Chem. Soc.*, 2010, **132**, 2160–2162.
  31. K. Tanaka and Y. Chujo, Recent progress of optical functional nanomaterials based on organoboron complexes with  $\beta$ -diketonate, ketoiminate and diiminate, *NPG Asia Mater.*, 2015, **7**, e223.
  32. Y. Chujo and K. Tanaka, New Polymeric Materials Based on Element-Blocks, *Bull. Chem. Soc. Jpn.*, 2015, **88**, 633–643.
  33. M. Gon, K. Tanaka and Y. Chujo, Recent progress in the development of

- advanced element-block materials, *Polym. J.*, 2017, **50**, 109–126.
34. M. Yamaguchi, S. Ito, A. Hirose, K. Tanaka and Y. Chujo, Luminescent color tuning with polymer films composed of boron diiminate conjugated copolymers by changing the connection points to comonomers, *Polym. Chem.*, 2018, **9**, 1942–1946.
  35. S. Ohtani, M. Gon, K. Tanaka and Y. Chujo, Construction of the Luminescent Donor–Acceptor Conjugated Systems Based on Boron-Fused Azomethine Acceptor, *Macromolecules*, 2019, **52**, 3387–3393.
  36. S. Ohtani, M. Gon, K. Tanaka and Y. Chujo, A Flexible, Fused, Azomethine–Boron Complex: Thermochromic Luminescence and Thermosalient Behavior in Structural Transitions between Crystalline Polymorphs, *Chem. Eur. J.*, 2017, **23**, 11827–11833.
  37. M. Gon, K. Tanaka and Y. Chujo, A Highly Efficient Near-Infrared-Emissive Copolymer with a N=N Double-Bond  $\pi$ -Conjugated System Based on a Fused Azobenzene-Boron Complex, *Angew. Chem. Int. Ed.*, 2018, **57**, 6546–6551.
  38. M. Yamaguchi, S. Ito, A. Hirose, K. Tanaka and Y. Chujo, Control of aggregation-induced emission *versus* fluorescence aggregation-caused quenching by bond existence at a single site in boron pyridinoiminate complexes, *Mater. Chem. Front.*, 2017, **1**, 1573–1579.
  39. A. Hirose, K. Tanaka, R. Yoshii and Y. Chujo, Film-type chemosensors based on boron diiminate polymers having oxidation-induced emission properties, *Polym. Chem.*, 2015, **6**, 5590–5595.
  40. S. Ito, K. Tanaka and Y. Chujo, Characterization and Photophysical Properties of a Luminescent Aluminum Hydride Complex Supported by a  $\beta$ -Diketiminato

- Ligand, *Inorganics*, 2019, **7**, 100.
41. S. Ito, A. Hirose, M. Yamaguchi, K. Tanaka and Y. Chujo, Size-discrimination of volatile organic compounds utilizing gallium diiminate by luminescent chromism of crystallization-induced emission via encapsulation-triggered crystal–crystal transition, *J. Mater. Chem. C*, 2016, **3**, 5564–5571.
  42. M. Yamaguchi, S. Ito, A. Hirose, K. Tanaka and Y. Chujo, Modulation of sensitivity to mechanical stimulus in mechanofluorochromic properties by altering substituent positions in solid-state emissive diiodo boron diiminates, *J. Mater. Chem. C*, 2016, **3**, 5314–5319.
  43. K. Suenaga, K. Tanaka and Y. Chujo, Heat - Resistant Mechanoluminescent Chromism of the Hybrid Molecule Based on Boron Ketoiminate Modified Octasubstituted Polyhedral Oligomeric Silsesquioxane, *Chem. Eur. J.*, 2017, **23**, 1409–1414.
  44. K. Suenaga, R. Yoshii, K. Tanaka and Y. Chujo, Sponge - Type Emissive Chemosensors for the Protein Detection Based on Boron Ketoiminate - Modifying Hydrogels with Aggregation - Induced Blueshift Emission Property, *Macromol. Chem. Phys.*, 2016, **217**, 414–417.
  45. K. Suenaga, K. Tanaka and Y. Chujo, Design and Luminescence Chromism of Fused Boron Complexes Having Constant Emission Efficiencies in Solution and in the Amorphous and Crystalline States, *Eur. J. Org. Chem.*, 2017, **2017**, 5191–5196.
  46. K. Suenaga, K. Uemura, K. Tananaka and Y. Chujo, Stimuli-responsive luminochromic polymers consisting of multi-state emissive fused boron ketoiminate *Polym. Chem.*, DOI: 10.1039/c9py01733j.

47. B. Ośmiałowski, A. Zakrzewska, B. Jędrzejewska, A. Grabarz, R. Zaleśny, W. Bartkowiak and E. Kolehmainen, Influence of Substituent and Benzoannulation on Photophysical Properties of 1-Benzoylmethyleneisoquinoline Difluoroborates, *J. Org. Chem.*, 2015, **80**, 2072–2080.
48. A. Zakrzewska, E. Kolehmainen, A. Valkonen, E. Haapaniemi, K. Rissanen, L. Chęcińska and B. Ośmiałowski, Substituent Effect in 2-Benzoylmethylenequinoline Difluoroborates Exhibiting Through-Space Couplings. Multinuclear Magnetic Resonance, X-ray Diffraction, and Computational Study, *J. Phys. Chem. A*, 2013, **117**, 252–256.
49. R. Zaleśny, N. A. Murugan, F. Gel'mukhanov, Z. Rinkevicius, B. Ośmiałowski, W. Bartkowiak and H. T. Ågren, Toward Fully Nonempirical Simulations of Optical Band Shapes of Molecules in Solution: A Case Study of Heterocyclic Ketoimine Difluoroborates, *J. Phys. Chem. A*, 2015, **119**, 5145–5152.
50. H. Qian, M. E. Cousins, E. H. Horak, A. Wakefield, M. D. Liptak and I. Aprahamian, Suppression of Kasha's rule as a mechanism for fluorescent molecular rotors and aggregation-induced emission, *Nat. Chem.*, 2017, **9**, 83–87.
51. D.-E. Wu, X.-L. Lu and M. Xia, Study on the solution and solid-state fluorescence of novel BF<sub>2</sub> complexes with (Z)-2-[phenanthridin-6(5H)-ylidene]-1-phenylethanone and its derivatives as ligands, *New J. Chem.*, 2015, **39**, 6465–6473.
52. Y. Wu, Z. Li, Q. Liu, X. Wang, H. Yan, S. Gong, Z. Liu and W. He, High solid-state luminescence in propeller-shaped AIE-active pyridine–ketoiminate–boron complexes, *Org. Biomol. Chem.*, 2015, **13**, 5775–5782.
53. Z. Zhang, P. Xue, P. Gong, G. Zhang, J. Peng and R. Lu,

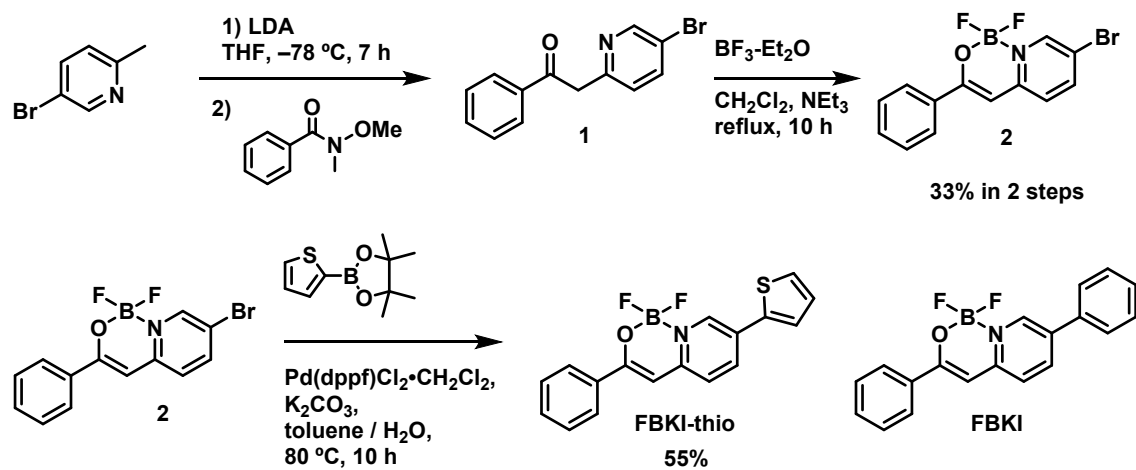


- Mechanofluorochromic behaviors of  $\beta$ -iminoenolate boron complexes functionalized with carbazole, *J. Mater. Chem. C*, 2014, **2**, 9543–9551.
54. A. Zakrzewska, R. Zaleśny, E. Kolehmainen, B. Ośmiałowski, B. Jędrzejewska, H. Ågren and M. Pietrzak, Substituent effects on the photophysical properties of fluorescent 2-benzoylmethylenequinoline difluoroboranes: A combined experimental and quantum chemical study, *Dyes Pigm.*, 2013, **99**, 957–965.
55. Q.-C. Yao, D.-E. Wu, R.-Z. Ma and M. Xia, Study on the structure–property relationship in a series of novel BF<sub>2</sub> chelates with multicolor fluorescence, *J. Organomet. Chem.*, 2013, **743**, 1–9.
56. M. Graser, H. Kopacka, K. Wurst, M. Ruetz, C. R. Kreutz, T. Müller, C. Hirtenlehner, U. Monkowius, G. Knör and B. Bildstein, Efficient fluorophores based on pyridyl-enolato and enamido difluoroboron complexes: Simple alternatives to boron-dipyrrromethene (bodipy) dyes, *Inorg. Chim. Acta*, 2013, **405**, 116–120.
57. M. Graser, H. Kopacka, K. Wurst, T. Müller and B. Bildstein, Structurally diverse pyridyl or quinolyl enolato/enamido metal complexes of Li, Zr, Fe, Co, Ni, Cu and Zn, *Inorg. Chim. Acta*, 2013, **401**, 38–49.
58. M. Gon, K. Tanaka and Y. Chujo, Concept of Excitation-Driven Boron Complexes and Their Applications for Functional Luminescent Materials, *Bull. Chem. Soc. Jpn.*, 2019, **92**, 7–18.
59. K. Tanaka, K. Nishino, S. Ito, H. Yamane, K. Suenaga, K. Hashimoto and Y. Chujo, Development of solid-state emissive o-carboranes and theoretical investigation of the mechanism of the aggregation-induced emission behaviors of organoboron “element-blocks”, *Faraday Discuss.*, 2017, **196**, 31–42.

60. R. Scaria, S. K. Dhawan and S. Chand, Synthesis of fluorene based two acceptor random copolymers for organic solar cell applications, *Synth. Met.*, 2014, **191**, 168–176.
61. R. Yoshii, K. Suenaga, K. Tanaka and Y. Chujo, Mechanofluorochromic Materials Based on Aggregation - Induced Emission - Active Boron Ketoiminates: Regulation of the Direction of the Emission Color Changes, *Chem. Eur. J.*, 2015, **21**, 7231–7237.
62. L. Wang, K. Wang, B. Zou, K. Ye, H. Zhang and Y. Wang, Luminescent chromism of boron diketonate crystals: distinct responses to different stresses, *Adv. Mater.*, 2015, **27**, 2918–2922.

## FIGURES AND TABLE

Scheme 1. Synthesis of FBKI-thio



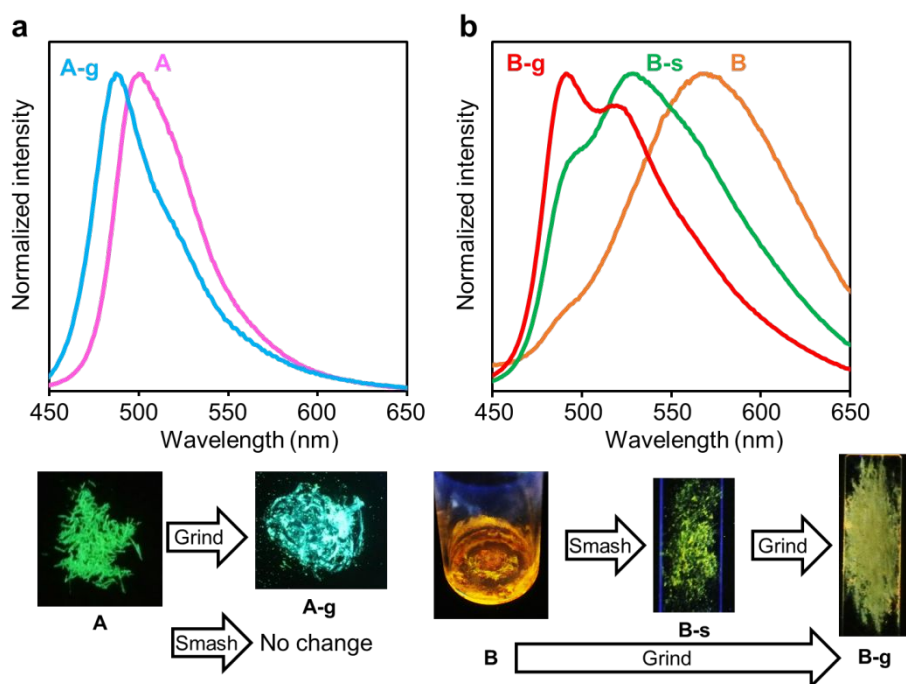


**Figure 1.** Appearances under UV irradiation (365 nm) and solid-state PL spectra of crystals (a) A and (b) B before and after the mechanical treatments with the excitation light at the absorption maximum wavelength (400 nm).

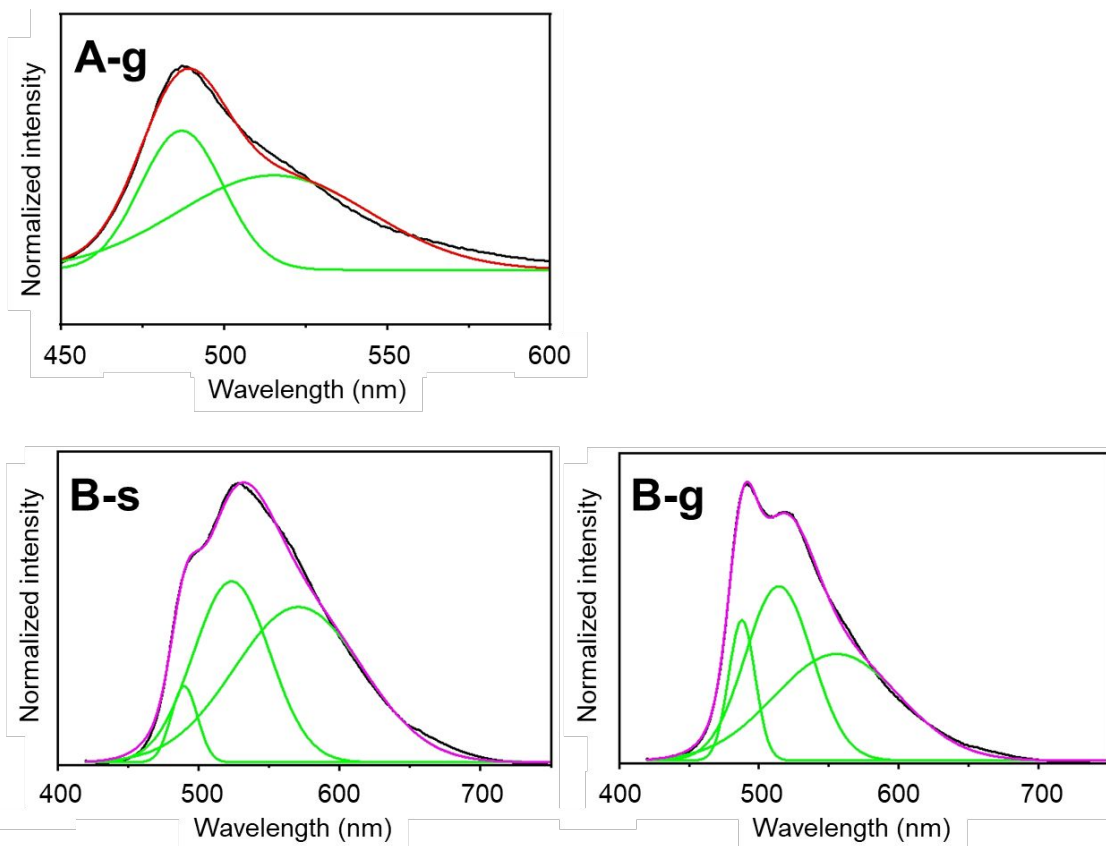


**Figure 2.** Peak deconvolution of emission spectra of FBKI-thio before and after the mechanical treatments.

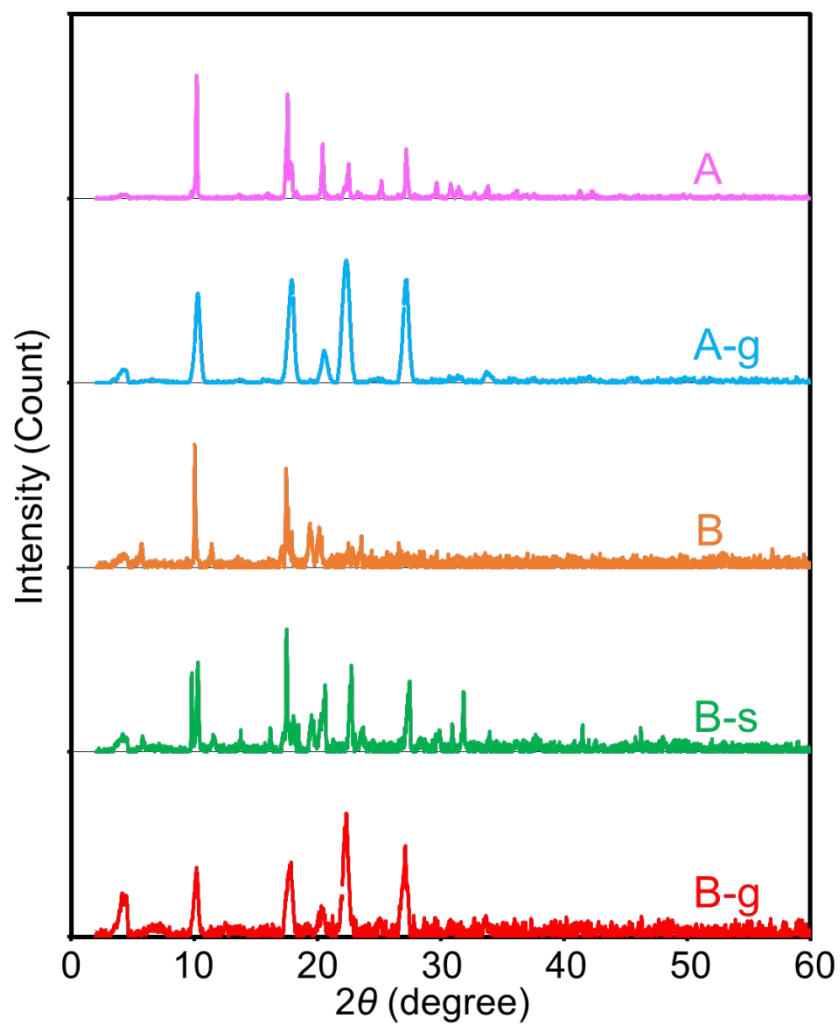


**Figure 3.** XRD patterns of FBKI-thio.

**Table 1.** Luminescent properties of FBKI-thio<sup>a</sup>

|                       | $\lambda_{\text{em}}$<br>(nm) | $\Phi_{\text{PL}}^b$ | $\tau_1$<br>(ns) <sup>c</sup> | $\tau_2$<br>(ns) <sup>c</sup> | $\tau_3$<br>(ns) <sup>c</sup> | $\chi^2$ |
|-----------------------|-------------------------------|----------------------|-------------------------------|-------------------------------|-------------------------------|----------|
| <b>A</b>              | 500                           | 0.20                 | 2.88<br>(40%)                 | 1.78<br>(60%)                 |                               | 1.07     |
| <b>A-g</b>            | 487                           | 0.15                 | 2.32<br>(39%)                 | 1.06<br>(61%)                 |                               | 1.12     |
| <b>B</b>              | 566                           | – <sup>d</sup>       | 1.64<br>(57%)                 | 0.65<br>(43%)                 |                               | 1.17     |
| <b>B-s</b>            | 529                           | 0.04                 | 4.34<br>(40%)                 | 1.84<br>(28%)                 | 0.54<br>(32%)                 | 1.04     |
| <b>B-g</b>            | 491                           | 0.03                 | 4.03<br>(32%)                 | 1.22<br>(36%)                 | 0.37<br>(32%)                 | 1.03     |
| Solution <sup>e</sup> | 466                           | 0.29                 | 0.93                          |                               |                               | 1.04     |

<sup>a</sup> Excited at  $\lambda_{\text{abs}}$  (400 nm) and 375 nm in static and kinetic measurements, respectively.

<sup>b</sup> Determined as an absolute value in the integration sphere.

<sup>c</sup> Detected at  $\lambda_{\text{em}}$ . Proportion of each component is shown in the parentheses.

<sup>d</sup> Not detectable due to fragility of the sample.

<sup>e</sup> Measured in THF ( $1.0 \times 10^{-5}$  M).

**Table 2.** Results of the peak deconvolution<sup>a</sup>

|            | $\lambda_1$ (nm) <sup>d</sup> | $\lambda_2$ (nm) <sup>d</sup> | $\lambda_3$ (nm) <sup>d</sup> | $A_1/A_2^b$ | $A_1/A_3^b$ | $A_2/A_3^b$ |
|------------|-------------------------------|-------------------------------|-------------------------------|-------------|-------------|-------------|
| <b>A</b>   | 501                           |                               |                               |             |             |             |
| <b>A-g</b> | 487<br>(39%)                  | 515<br>(61%)                  |                               | 0.63        |             |             |
| <b>B</b>   | 566                           |                               |                               |             |             |             |
| <b>B-s</b> | 490<br>(6%)                   | 523<br>(39%)                  | 570<br>(56%)                  | 0.15        | 0.10        | 0.69        |
| <b>B-g</b> | 488<br>(13%)                  | 514<br>(41%)                  | 556<br>(46%)                  | 0.32        | 0.28        | 0.87        |

<sup>a</sup> Proportion of peak area is shown in parentheses.

<sup>b</sup> Calculated with the peak areas.



## GRAPHICAL ABSTRACT

